Electronic Supplementary Material (ESI) for Dalton Transactions.

Magnetic behavior of the novel pentagonal-bipyramidal Erbium(III) complex $(Et_3NH)[Er(H_2DAPS)Cl_2]$: high-frequency EPR study and crystal-field analysis

L. Spillecke and C. Koo

Kirchhoff Institute for Physics, Heidelberg University, INF 227, D-69120, Heidelberg, Germany

O. Maximova

Lomonosov Moscow State University, Moscow 119991, Russia

A. N. Vasiliev

Lomonosov Moscow State University, Moscow 119991, Russia and National University of Science and Technology "MISiS", Moscow 119049, Russia

V. S. Mironov

Shubnikov Institute of Crystallography of Federal Scientific Research Centre 'Crystal-lography and Photonics', RAS, Moscow, Russia and Institute of Problems of Chemical Physics, RAS, Chernogolovka 142432, Russia

D. V. Korchagin, V. A. Kopotkov, and E. B. Yagubskii

Institute of Problems of Chemical Physics, RAS, Chernogolovka 142432, Russia

R. Klingeler

Kirchhoff Institute for Physics, Heidelberg University, INF 227, D-69120, Heidelberg, Germany and Centre for Advanced Materials (CAM), Heidelberg University, Germany

Table S 1. Selected bond lengths (Å) and bond angles (º) of **1**.

Er(1)-O(5)	2.246(3)
Er(1)-O(5)$^{\#1}$	2.246(3)
Er(1)-N(1)	2.424(4)
Er(1)-N(1)$^{\#1}$	2.424(4)
Er(1)-N(2)	2.425(6)
Er(1)-Cl(1)	2.586(2)
Er(1)-Cl(2)	2.654(2)
O(5)$^{\#1}$-Er(1)-O(5)	96.0(2)
O(5)-Er(1)-N(2)	131.97(8)
O(5)-Er(1)-N(1)	66.5(1)
O(5)-Er(1)-N(1)$^{\#1}$	162.4(1)
N(1)-Er(1)-N(2)	65.54(9)
O(5)-Er(1)-Cl(1)	94.81(9)
N(1)$^{\#1}$-Er(1)-N(1)	131.1(2)
N(1)$^{\#1}$-Er(1)-N(2)	65.54(9)
N(2)-Er(1)-Cl(1)	84.7(1)
N(1)-Er(1)-Cl(1)	87.76(9)
O(5)-Er(1)-Cl(2)	94.42(8)
N(2)-Er(1)-Cl(2)	81.5(1)
N(1)-Er(1)-Cl(2)	86.54(9)
Cl(1)-Er(1)-Cl(2)	166.19(5)

Symmetry transformations used to generate equivalent atoms: $^{\#1}$ -x-2, y, z

Table S 2. The deviation geometric parameters as calculated from the Continuous Shape Measures by *SHAPE* program for different probable coordination geometries with seven coordination number around the Er centers.

Ln	PBPY-7	JPBPY-7	CTPR-7	COC-7	JETPY-7	HPY-7	HP-7
Er (**1**)	**1.031**	6.505	7.280	9.054	24.543	25.231	33.748

PBPY-7: Pentagonal bipyramid (D_{5h}), COC-7 Capped octahedron* (C_{3v}), CTPR-7 Capped trigonal prism * (C_{2v}), JPBPY-7 Johnson pentagonal bipyramid (J13) (D_{5h}), JETPY-7 Elongated triangular pyramid (J7) (C_{3v}), HPY-7 Hexagonal pyramid (C_{6v}), HP-7 Heptagon (D_{7h})

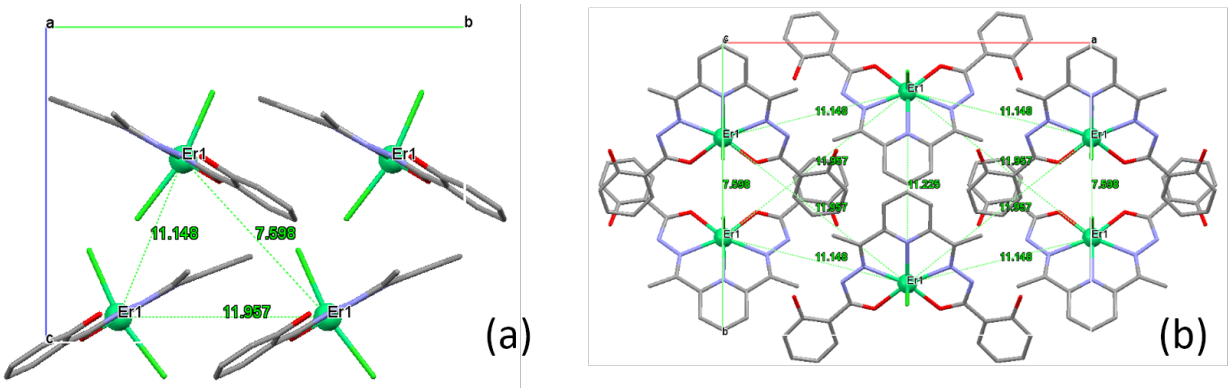

Figure S 1. Unit cell contents in the crystal packing of **1** along crystallographic a (left) and c (right) axes. The inter Er-Er of the neighbour molecules are shown by green dashed lines (values are in Å). The Et_3NH counter cations and H atoms are omitted for clarity.

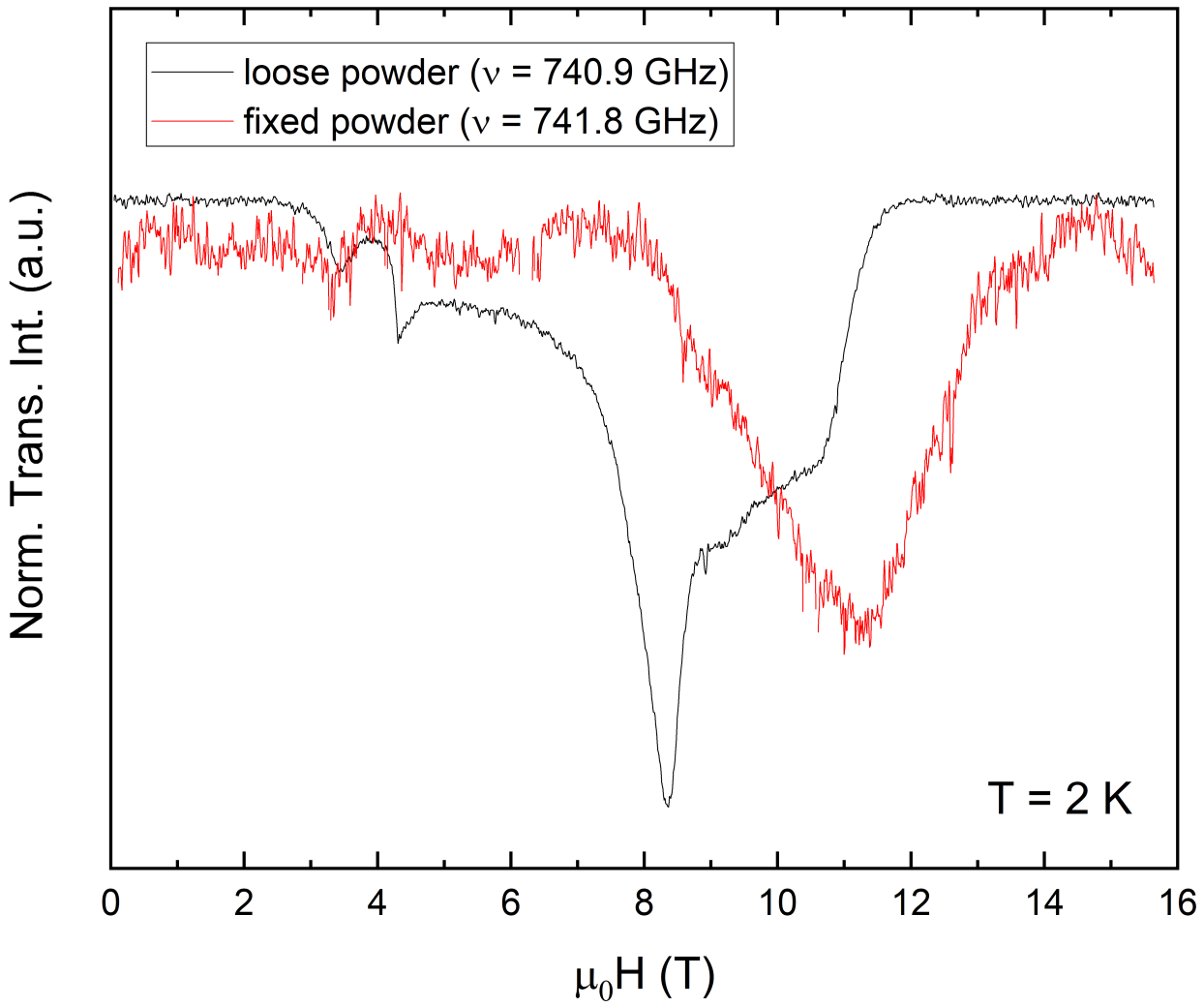

Figure S 2. HF-EPR spectra measured on a loose and a fixed powder sample, respectively, at almost the same frequency. For the fixed powder sample, spectral weight is shifted to higher fields and the resonance maximum is at the position of the shoulder-like feature of the loose powder spectra. We conclude: (1) The shoulder-like feature in the loose powder sample is arising from a small amount of crystallites which are not perfectly aligned. (2) The obvious differences between the spectral shape obtained for loose and fixed powder samples unambiguously show, that an alignment of the crystallites within the external magnetic field was successful for the majority of the loose powder.

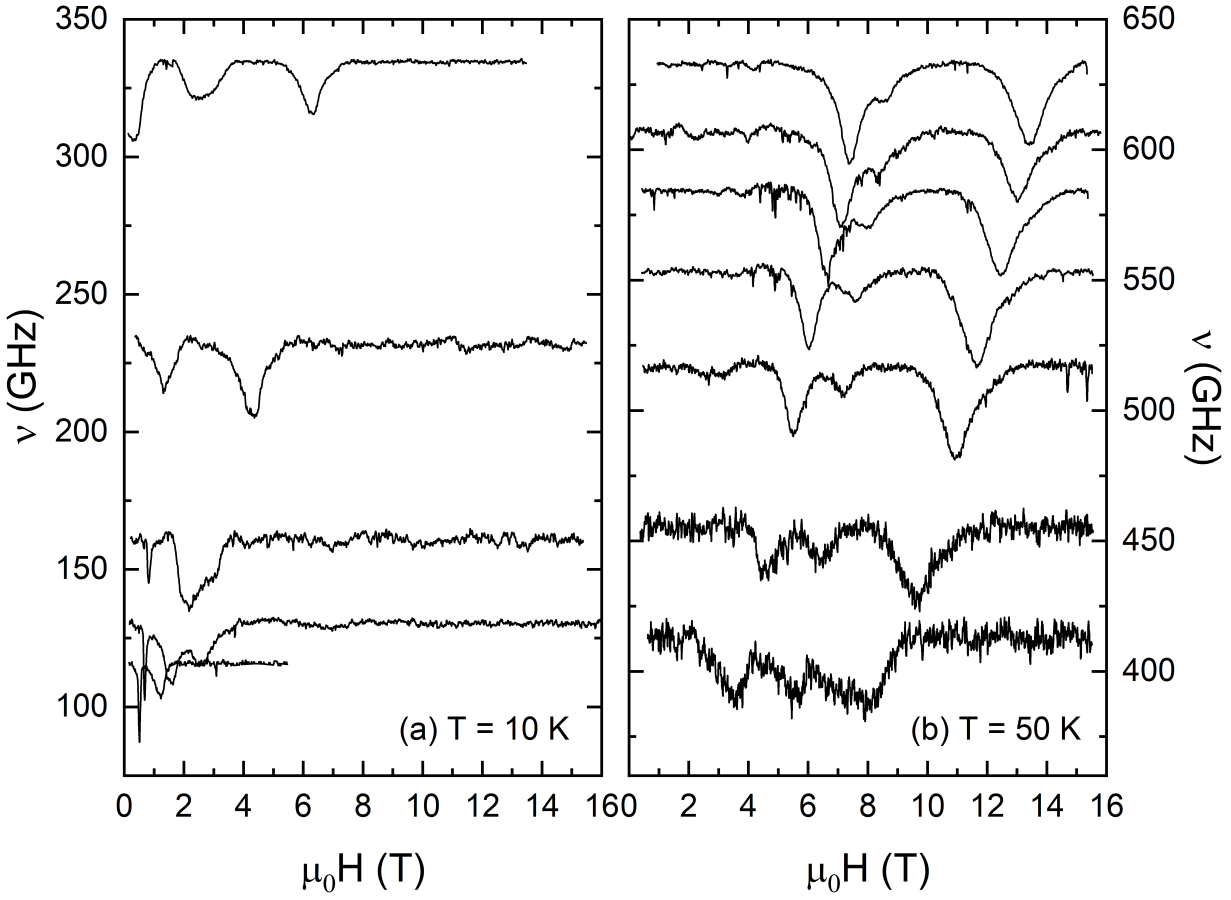

Figure S 3. HF-EPR spectra obtained at a fixed temperature of (a) $T = 10$ K and (b) $T = 50$ K. The spectra are vertically shifted so that the minimum of each spectra coincides with the measurement frequency.

Table S 3. Calculated crystal-field parameters B_{kq} (in cm^{-1}) for Er(III) ions in complex 1. Real (Re) and imaginary (Im) parts of complex B_{kq} parameters are indicated.

k	q	ReB_{kq}	ImB_{kq}
2	0	118.6	0
2	1	0	0.1
2	2	27.1	0.2
4	0	1207.7	0
4	1	-0.1	38.4
4	2	-83.6	-0.5
4	3	0	4.3
4	4	-213.3	-2.7
6	0	-10.1	0
6	1	0	10.1
6	2	9.7	0
6	3	0	-4.9
6	4	156.3	2
6	5	0.2	-13.8
6	6	-284.0	-5.5
$S^{(a)}$, cm^{-1}			439.8

$^{(a)}$ The S criterion estimates the overall strength of the crystal-field potential of Ln3+ ions in terms of B_{kq} parameters,[1]

$$S = \left[\frac{1}{3}\sum_{k=2,4,6}\left(\frac{1}{2k+1}\right)\left(\mathbf{Re}B_{kq}^2 + \mathbf{Im}B_{kq}^2\right)\right]^{\frac{1}{2}} \quad (1)$$

[1] N. C. Chang, J. B. Gruber, R. P. Leavitt, and C. A. Morrison, The Journal of Chemical Physics **76**, 3877 (1982).

Table S 4. Calculated JM composition of wave functions of the three lowest crystal-field states KD1, KD2 and KD3 of Er(III) ions in complex **1**.

CF state	Energy (cm^{-1})	JM composition of wave function
KD1	0	$0.57\|\pm 9/2\rangle + 0.15\|\mp 7/2\rangle + 0.11\|\mp 3/2\rangle$
KD2	9.0	$0.65\|\pm 11/2\rangle + 0.12\|\mp 9/2\rangle + 0.11\|\pm 7/2\rangle$
KD3	22.0	$0.36\|\pm 7/2\rangle + 0.22\|\mp 5/2\rangle + 0.18\|\pm 11/2\rangle$

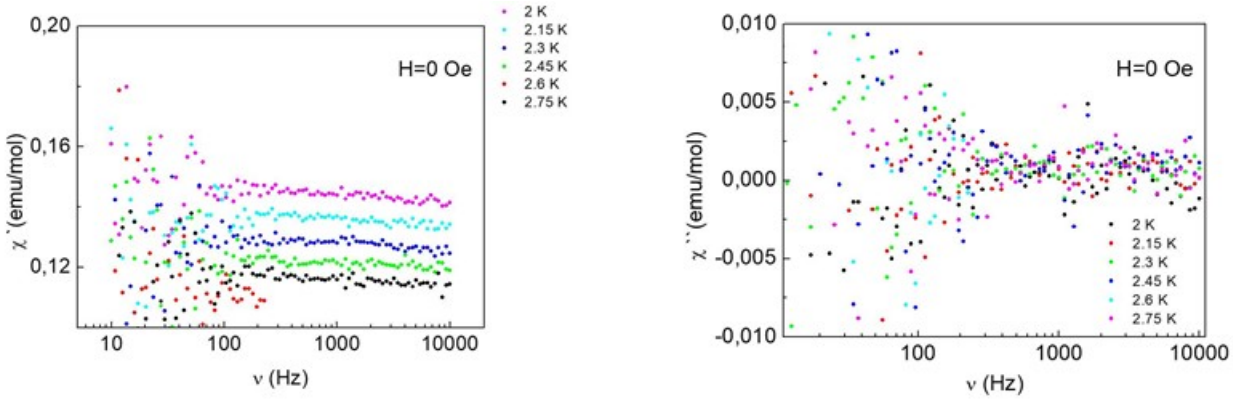

Figure S 4. Frequency dependence of the in-phase (χ') and out-of-phase ac magnetic susceptibility (χ") of **1** at 2 K – 3.8 K and $H_{DC} = 0$ T.

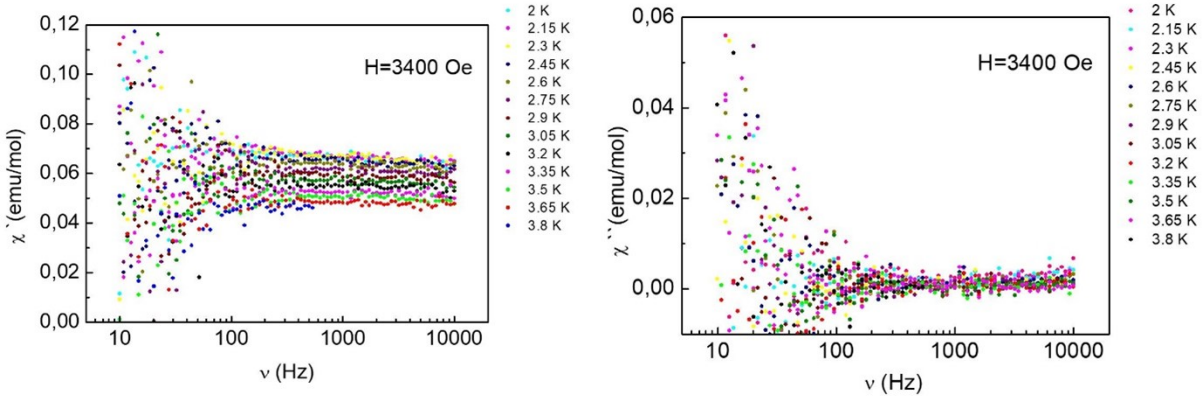

Figure S 5. Frequency dependence of the in-phase (χ') and out-of-phase ac magnetic susceptibility (χ") of **1** at 2 K – 3.8 K and $H_{DC} = 0.34$ T.

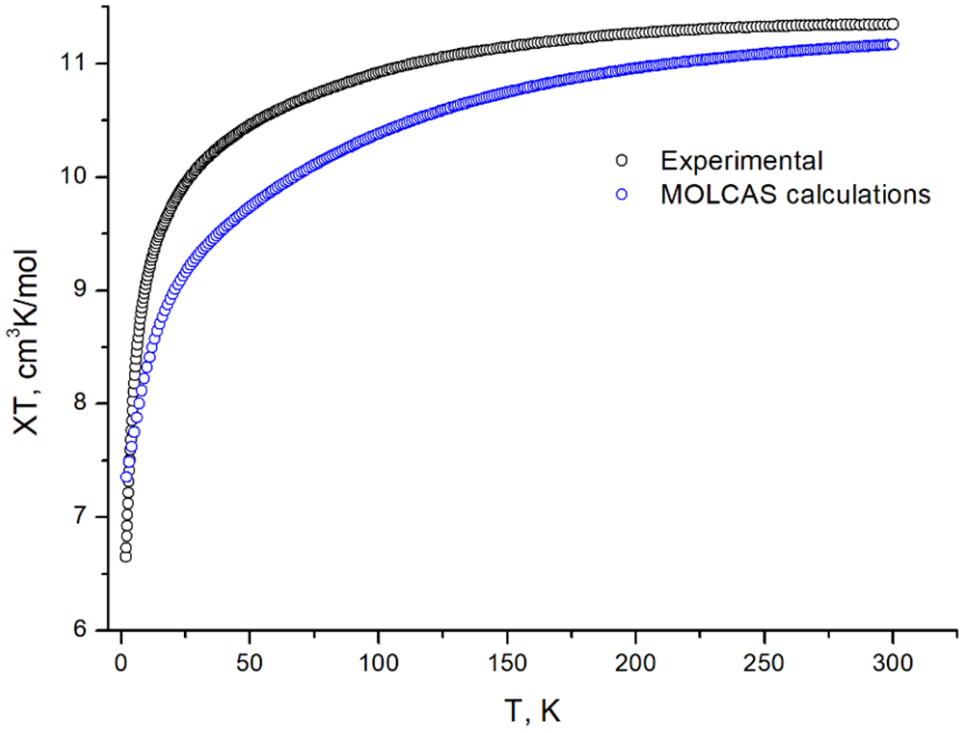

Figure S 6. Comparison between the experimental magnetic susceptibility of **1** ($E_{\mathrm{CF}} = 245$ cm^{-1}) and magnetic susceptibility obtained from ab initio CASSCF/RASSI+SO/SINGLE_ANISO calculations for isolated complex $[\mathrm{Er}(\mathrm{H_2DAPS})\mathrm{Cl_2}]^-$ with OpenMolcas program ($E_{\mathrm{CF}} = 423$ cm^{-1}).

Table S 5. SINGLE_ANISO computed JM composition of wave functions of the CF states of the lowest $^4I_{15/2}$ multiplet of Er(III) ion in complex $[Er(H_2DAPS)Cl_2]^-$.

CF state, Energy (cm^{-1})	JM composition of wave functions (main contributions)
0.00	$0.519\|\pm15/2\rangle + 0.371\ \|\pm11/2\rangle + 0.104\ \|\pm7/2\rangle$
26.24	$0.458\|\pm9/2\rangle + 0.350\|\pm5/2\rangle + 0.074\|\pm7/2\rangle +$ $0.050\|\pm13/2\rangle + 0.048\|\pm3/2\rangle$
60.15	$0.649\|\pm7/2\rangle + 0.124\|\pm9/2\rangle + 0.079\|\pm3/2\rangle +$ $0.050\ \|\pm1/2\rangle + 0.044\ \|\pm15/2\rangle + 0.034\|\pm11/2\rangle$
159.71	$0.526\|\pm5/2\rangle + 0.286\|\pm9/2\rangle + 0.079\|\pm7/2\rangle +$ $0.064\|\pm3/2\rangle + 0.025\|\pm13/2\rangle$
199.31	$0.601\|\pm3/2\rangle + 0.155\|\pm1/2\rangle + 0.108\|\pm5/2\rangle +$ $0.092\ \|\pm7/2\rangle + 0.028\|\pm9/2\rangle$
281.43	$0.755\|\pm1/2\rangle + 0.192\|\pm3/2\rangle + 0.035\|\pm13/2\rangle$
399.21	$0.879\|\pm13/2\rangle + 0.098\|\pm9/2\rangle$
423.48	$0.578\|\pm11/2\rangle + 0.396\|\pm15/2\rangle$

Table S 6. Crystal-field energies (cm^{-1}), g-tensors and JM composition of wave functions of Er(III) ion calculated with use of the leading axial CF parameter B_{40} = 1207 cm^{-1} (see Table S3) and zero other B_{kq} parameters.

Energy (cm^{-1})	g_x	g_y	g_z	JM composition of wave function
0	0.000	0.000	13.156	$\|\pm11/2\rangle$
8.2	0.000	0.000	10.764	$\|\pm9/2\rangle$
49.0	0.000	0.000	8.372	$\|\pm7/2\rangle$
53.1	0.000	0.000	15.549	$\|\pm13/2\rangle$
99.7	0.000	0.000	5.980	$\|\pm5/2\rangle$
143.0	0.000	0.000	3.588	$\|\pm3/2\rangle$
167.5	9.568	9.568	1.196	$\|\pm1/2\rangle$
209.1	0.000	0.000	17.941	$\|\pm15/2\rangle$

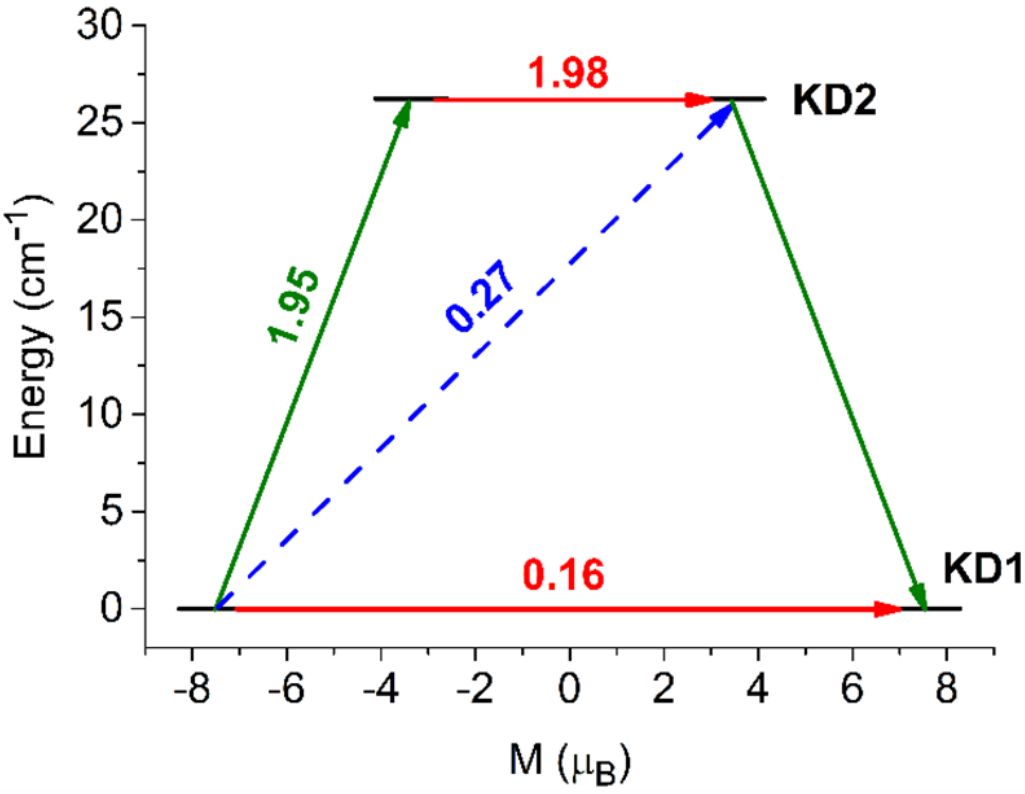

Figure S 7. Computed possible magnetization relaxation pathways of Er(III) ions in **1**. The red arrows show the QTM and TA-QTM via ground and higher excited KD, respectively. The blue arrow shows the Orbach process for the relaxation. The green arrows show the mechanism of magnetic relaxation.

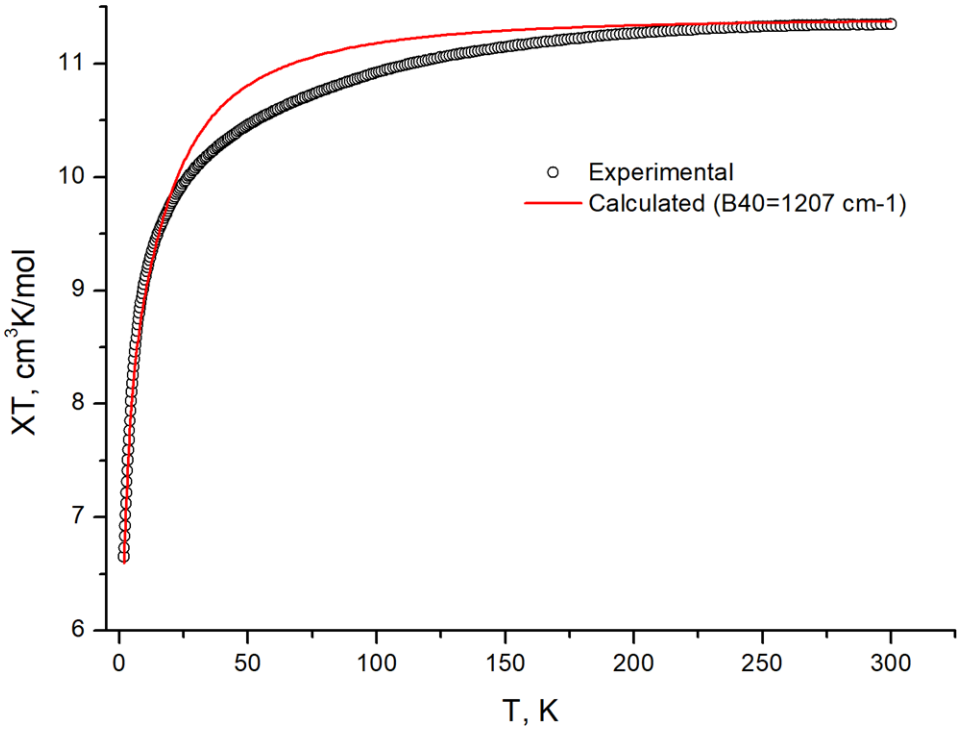

Figure S 8. Comparison between the experimental magnetic susceptibility of **1** and magnetic susceptibility obtained from CF calculations for Er(III) ion with use of the leading axial CF parameter $B_{40} = 1207$ cm^{-1} (see Table S3) and zero other B_{kq} parameters.

Table S 7. Crystal-field energies (in K), g-tensors and JM composition of wave functions of Dy(III) ion in complex $[Dy(H_2DAPS)Cl_2]^-$ calculated with the set of CF parameters B_{kq} obtained for Er(III) ion in complex $[Er(H_2DAPS)Cl_2]^-$ (Table S3).

CF state Energy (K)	g_x	g_y	g_z	JM composition of wave function
0	0.034	0.075	19.743	$0.989\|\pm 15/2\rangle$
138.4	1.306	6.856	13.652	$0.924\|\pm 1/2\rangle + 0.037\|\pm 3/2\rangle + 0.013\|\pm 13/2\rangle$
180.3				
234.8				
314.5				
379.0				
417.1				
437.7				